RSC Advances

PAPER

View Article Online
View Journal | View Issue

Cite this: *RSC Adv.*, 2016, **6**, 6251

Outstanding dielectric constant and piezoelectric coefficient in electrospun nanofiber mats of PVDF containing silver decorated multiwall carbon nanotubes: assessing through piezoresponse force microscopy

Maya Sharma,[a] Vijay Srinivas,[b] Giridhar Madras[c] and Suryasarathi Bose*[b]

In order to enhance the piezoelectric β-phase, PVDF was electrospun from DMF solution. The enhanced β-phase was discerned by comparing the electrospun fibers against the melt mixed samples. While both the processes resulted in phase transformation of α- to electroactive β-polymorph in PVDF, the fraction of β-phase was strongly dependent on the adopted process. Two different nanoscopic particles: carboxyl functionalized multiwall carbon nanotubes (CNTs) and silver (Ag) decorated CNTs were used to further enhance the piezoelectric coefficient in the electrospun fibers. Fourier transform infrared spectroscopy (FTIR) and wide-angle X-ray diffraction (XRD) supports the development of piezoelectric β-phase in PVDF. It was concluded that electrospinning was the best technique for inducing the β-polymorph in PVDF. This was attributed to the high voltage electrostatic field that generates extensional forces on the polymer chains that aligns the dipoles in one direction. The ferroelectric and piezoelectric measurement on electrospun fibers were studied using piezo-response force microscope (PFM). The Ag–CNTs filled PVDF electrospun fibers showed the highest piezoelectric coefficient (d_{33} = 54 pm V^{-1}) in contrast to PVDF/CNT fibers (35 pm V^{-1}) and neat PVDF (30 pm V^{-1}). This study demonstrates that the piezoelectric coefficient can be enhanced significantly by electrospinning PVDF containing Ag decorated nanoparticles.

Received 2nd December 2015
Accepted 4th January 2016

DOI: 10.1039/c5ra25671b

www.rsc.org/advances

1. Introduction

In the last few years, electrospinning of polymers to produce nanofibers has progressively gained popularity for its varied range of properties and applications involving semi-permeable membranes for water filtration,[1,2] polymer composite reinforcement,[3] fuel cell applications,[4] drug delivery,[5] biosensors,[4] scaffolds for tissue engineering[6–8] and other applications. The nanofibers thus produced through different methods often pave way for better performance as compared to filled composites. PVDF [poly(vinylidene fluoride)] is a semi crystalline polymer and exhibits excellent piezo- and ferroelectric properties. PVDF exists in five crystalline phases – α, β, γ, δ and ε, of which α and β are the predominant phases.[9,10] The α phase has TGTG′ semi-helical conformation and it is the most stable polymorph that develops upon cooling from melt. The electroactive β-polymorph is polar and is commercially relevant in context to its piezoelectric properties. The β phase exists in *trans*-conformation *i.e.* H and F are on the opposite side of the main backbone chain, resulting in non-zero dipole moment in PVDF.

Various strategies have been employed in the past for obtaining the β phase such as drawing or uniaxial stretching,[11–13] thermal annealing,[14] high electric field[15] and mechanical rolling.[16] Apart from processing, incorporation of nanoparticles also induces β phase in PVDF.[17,18] Due to the *trans*-(TTTT) structure in the main chain, the dipole moment per unit cell is highest for the β phase that leads to high piezoelectric properties. PVDF composites have been extensively investigated because of their excellent properties like ionic conductivity, good mechanical properties, electrochemical stability and piezoelectric properties.[19,20] Because of inertness, high thermal and mechanical properties, PVDF is being used for the water filtration membranes.[1,21] The piezo- and pyroelectric properties make PVDF attractive for energy conversion applications like electromechanical actuators, micro electric-mechanical devices, and energy harvesters.[22–24] Recently, silver nanoparticles have attracted a great deal of interest in the context of imparting piezoelectric behavior in PVDF based composites.[25,26] It has been reported that an

[a]*Center for Nano Science and Engineering, Indian Institute of Science, Bangalore-560012, India*

[b]*Department of Materials Engineering, Indian Institute of Science, Bangalore-560012, India. E-mail: sbose@materials.iisc.ernet.in*

[c]*Department of Chemical Engineering, Indian Institute of Science, Bangalore-560012, India*

electrostatic interaction between the CF_2 dipole and the charges present on the Ag nanoparticle causes the PVF_2 chains to become straightened that leads to the formation of the zigzag conformation of β polymorph instead of the coiled α conformation.[26] The good piezoelectric properties and high aspect ratio of Ag nanoparticles make them attractive candidates as fillers in the PVDF matrix.

Apart from the aforementioned techniques, electrospinning is also an important technique to induce β phase in PVDF. Many groups have studied the properties of electrospun PVDF fibers, and a handful of these studies have reported on the optimization, characterization and properties of electrospun PVDF and PVDF fibers containing various nanoparticles.[27–32] In a typical electrospinning process, PVDF dipoles are naturally aligned within the crystals pointing in a single direction. This occurs because the high voltage electrostatic field generates extensional forces that act on the polymer chains and aligned the dipoles in one direction. Using high voltage, electrospinning can be used to produce 1D continuous nano dimensional fibers. Various parameters including the solvent used for electrospinning, conditions like humidity and temperature, voltage, flow rate, working distance and concentration affect the electrospun fiber mats and its subsequent properties.[33,34]

In the present study, we have compared PVDF and PVDF based composites prepared by melt mixing and electrospinning with respect to dielectric and piezoelectric behavior. We have demonstrated the effect of different processes on the formation of β-phase in PVDF. Two different nanoscopic particles: carboxyl functionalized CNTs and Ag decorated CNTs were used to enhance the piezoelectric coefficient in the electrospun fibers. Fourier transform infrared spectroscopy (FTIR) and wide-angle X-ray diffraction (XRD) was used to understand the development of piezoelectric β-phase in PVDF. The ferroelectric and piezoelectric properties of the electrospun fibers were systematically studied using piezoresponse force microscope (PFM).

2. Experimental

2.1 Materials

Commercial grade PVDF with M_w of 440 000 g mol^{-1} (Kynar-761) was procured from Arkema Inc. Silver nitrate ($AgNO_3$) was procured from Sigma Aldrich. The carboxyl acid functionalized multiwalled carbon nanotubes (CNTs) were obtained from Nanocyl (Belgium).[35] All solvents used were of analytical grade and procured from S.D. Fine chemicals (India).

2.2 Synthesis of Ag decorated MWNTs

For decorating Ag onto the carboxyl acid functionalized MWNTs, we adopted a procedure that has been discussed earlier.[36] The –SH groups were first introduced onto the MWNTs. Briefly, to produce the thiolated MWNTs, the acid-functionalized MWNTs were dispersed in THF, and NaSH aqueous solution was added[21] and stirred at 50 °C for 12 h. The thiolated MWNTs were further dispersed in DI water in which 0.15 M $AgNO_3$ solution was added drop wise under vigorous stirring. 0.1 M NaOH solution was added drop wise (to maintain the pH of 6.3) and stirred for 20 h (Scheme 1). The Ag–CNT nanoparticles were separated by centrifugation, washed twice with DI water, and then vacuum dried.

2.3 Electrospinning of PVDF PVDF/CNTs, PVDF/Ag–CNT fibers

A needle based electrospinning setup was employed to prepare PVDF nanofiber mats. For optimization of electrospinning process, we varied various parameters like PVDF, solvent (DMF/acetone) (v/v) concentration *etc.* During electrospinning, a controlled flow rate was maintained at 0.5 ml h^{-1} for the prepared solutions. This flow rate was chosen because the electrospinning process under this condition was stable regardless of the variation of other parameters studied. The thickness of fiber mats was controlled by the deposition time of the electrospinning process. The spinning process was conducted at room temperature and all the electrospun nanofiber mats were then dried in an oven at 40 °C for 5 h to remove the residual solvent. For optimization of the PVDF fiber mat, PVDF was dissolved in different ratios in DMF/acetone in various concentrations to obtain non-beaded fibers. PVDF fiber mats were electrospun from a polymer solution containing various concentrations (10, 16, 25, and 40%) in different ratio of DMF/acetone [(2/8), (3/7) and (5/5)] were prepared. The following processing conditions: working distance of 15 cm, volume feed rate of 0.5 ml h^{-1} and high-voltage power supply of 15 kV were used for preparing the fiber mats. 25 wt% PVDF in 1/1 ratio of DMF/acetone gave the best fibers in contrast to other concentrations. At concentrations below 20 wt% of PVDF in the solution, beaded fibers were noted because of low viscosity of the solution.

Many groups have investigated the effect of polymer concentration on the fiber morphology and its properties.[37–39] For instance, increasing the polymer concentration from 10 to 25 wt% (PVDF), the morphology changes dramatically from

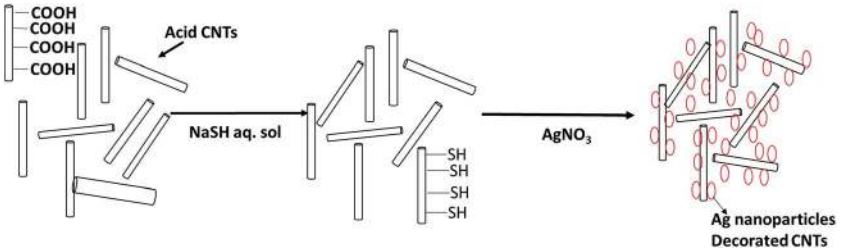

Scheme 1 Preparation of Ag decorated CNTs from acid functionalised CNTs.

a beaded morphology to non-beaded fibers. The increase in the viscosity of the solution leads to an increase in the entanglement in the polymer chains that helps in the stretching of the fibers on account of charge during electrospinning.[40] For further preparation of various fiber containing different nanoparticles, the concentration of PVDF in the solution was fixed at 25 wt%. At this concentration, the solution conductivity is high enough and more charges can be carried by the electrospinning jet. The increased charge carried by the solution increase the stretching of the fibers. However, when the polymer concentration is very high, it is difficult to electrospun because at high viscosity, the polymer solution will be dry before it hits the collector plate.

As one of the rationale behind this study was to develop good fibers, various parameters were optimized. For the preparation of CNTs and Ag decorated CNTs incorporated PVDF fiber mats, 10 mg of nanoparticles were taken in a glass vial and was dispersed in 1 : 1 DMF/acetone solution using bath sonication followed by probe sonication to ensure proper dispersion of the particles. 0.99 g of PVDF was later added to the solution and was heated at 40 °C for 10 min to dissolve the polymer in the solution. Later, the solution was loaded onto a syringe pump the flow rate was (0.5 ml h^{-1}), thereby producing a Tylor cone. A voltage of 15 kV, and a syringe tip-to plate collector distance of 16 cm and a flow rate of 0.5 ml h^{-1} was optimized for the PVDF/CNTs and for the PVDF/Ag–CNTs solution. A 16 gauge (G) needle was used for spinning PVDF/Ag–CNTs solution to prevent the clogging of Ag–CNTs in a 25 G needle (which was used for PVDF fibers). In all the above mentioned fibers, the concentration of the polymer (25 wt%) and the nanoparticles (1 wt%) were fixed and all the fibers were optimized separately.

2.4 Preparation of melt mixed composites

For comparison, different PVDF composites were prepared by melt blending using HAAKE extruder CTWS at 220 °C for 20 min with a screw speed of 60 rpm. Melt mixing was carried out under N_2 atmosphere to prevent oxidative degradation. The concentration of the particles were fixed similar to those of the electrospun fibers.

2.5 Characterization of nanoparticles

The XRD scans of nanoparticles were recorded using a PANalytical X'Pert Pro using a Cu Kα radiation (40 kV) in the 2θ range of 10–900° and a scan rate of 0.04° s^{-1}. For morphology and diffraction of nanoparticles, TEM (Tecnai G2 T20) was used and operated at 200 kV. TEM samples were prepared using solution casting method on a holey carbon coated copper grid using very dilute solutions. The atomic concentration and the elemental mass conc. of Ag in Ag–CNTs are 0.65% and 4.24% (determined apriori from atomic absorption spectra, AAS and X-ray photoelectron spectroscopy, (XPS), not shown here).

2.6 Characterization of melt mixed samples and electrospun fibers

Perkin-Elmer frontier was used for recording FTIR spectra of the fiber mats by accumulating 32 scans with a resolution of 2 cm^{-1} over a range of 600–4000 cm^{-1}. For evaluating different phases in PVDF, XRD scans were recorded using a PANalytical X'Pert Pro using a Cu Kα radiation. For ferroelectric and piezoelectric measurements, Bruker AFM in piezo-mode was used. AFM tip ($K = 3$ N m^{-1} and $F = 75$ kHz) from Budget sensors was used to conduct ferroelectric measurements. Polarization and amplitude curves were measured at 100 Hz and up to 10 V. For AFM piezoresponse measurements, we first scan a 20 × 20 μm area and calculate piezoresponse at each point using measured total deflection and applied electric field. We take average of d_{33} obtained at various different points. We repeated this measurement at least five places with same area and parameters.

3. Results and discussion

3.1 Characterization of Ag decorated CNTs

The micro-structure of Ag decorated CNTs was obtained and analyzed using XRD and TEM (Fig. 1). The XRD scans of Ag–CNTs show the characteristic peaks of Ag at 45° for (200) plane and at *ca.* 65° (2θ) for (220) plane. The CNT peak (002) is clearly visible at *ca.* 27°. Fig. 1b clearly shows Ag particles decorated on the walls of the carbon nanotubes and the average sizes of the Ag particles obtained from the TEM image are *ca.* 10 nm. The TEM and XRD analysis clearly show that the Ag is well decorated onto the CNTs.

3.2 Morphology of different fibers mats

Fiber morphology was analysed using SEM (Fig. 2). From SEM, we can clearly see that the fibers were free of beads. Few wrinkles were observed on the surfaces of all the fibers, as observed in high-resolution SEM images (Fig. 2d and e). It is reported that wrinkles, pores and raised areas in PVDF fibers is usually formed in a mixed solvent system with high acetone content.[32,41] The surface roughness is higher in PVDF/Ag–CNTs as compared to PVDF fibers. A thread like morphology was also observed on the surface of PVDF/Ag–CNTs fibers, possibly due to the presence of CNTs in the fibers.[42] PVDF chains and CNTs presumable align along the poling and stretching direction[31] that can lead to β-phase in electrospun PVDF fibers. It has been reported that dispersed CNTs were randomly oriented in the electrospinning solution, but they were aligned along the flow direction at the Taylor cone.[32] Moreover, due to the elongation of the fluid during jet travel, the nanotubes were further spread out along

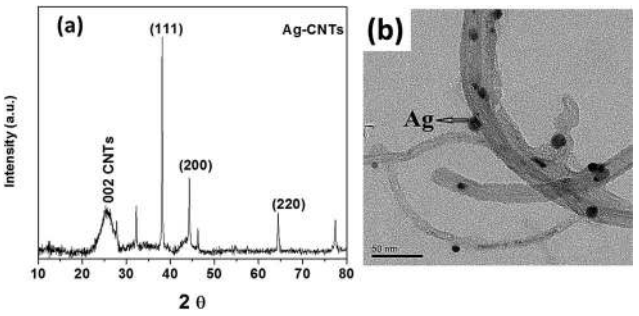

Fig. 1 (a) XRD scan of Ag–CNTs (b) transmission electron microscopy of Ag–CNTs.

the direction of motion of the jet and can lead to high conductivity in the fibers. Interestingly, no beads were observed in PVDF/CNTs fibers indicating proper dispersion of CNTs in the polymer matrix.[43] Poor dispersion of CNTs in the polymer matrix often lead to structural irregularity in the electrospun fibers[44] and can lead to the formation of beads with different structural inhomogeneity in the fibers.

The SEM results indicate that the average diameter of PVDF fibers (*ca.* 1.5 μm) are higher than PVDF/CNTs (*ca.* 300 nm) and PVDF/CNTs fibers (*ca.* 500 nm). This is probably due to increase in conductivity of spin dope by the addition of CNTs.[45] It is worth mentioning here that the difference in PVDF fibre diameter is not due to different syringes used in this study. We tried both 16 and 25 G needles for PVDF fibres. Both the syringes produced almost similar fibre morphology. The decrease in fibre diameter with addition of nanoparticles can be attributed to the proper dispersion of CNTs in the polymer matrix because the repulsive forces generated by CNTs could alleviate the chain entanglement of PVDF macromolecules.[45] The fiber diameter for different fibers mats are shown in Fig. 3. The fibre diameter using the 16 G needle varied in the range of 1.3–1.9 μm; similar to the diameter obtained using the 25 G needle. However, the fiber diameter slightly increases with the addition of Ag–CNTs in the PVDF spin dope. This can be attributed to the increase in viscosity that has a greater impact on fibre diameter than a slight increase in the electrical conductivity.[43] In addition, it is worthwhile to note that the PVDF fibers obtained using either 16 G or 25 G needle exhibited similar β fraction. Hence, this allows us to compare the β fraction of different diameter fibers.

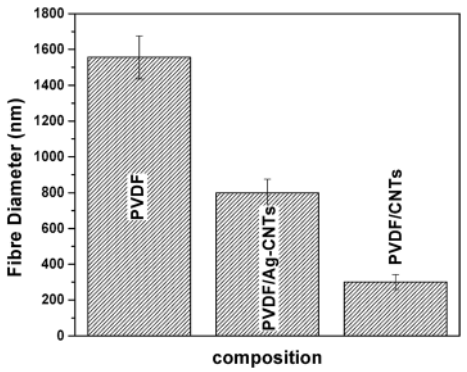

Fig. 3 Fiber diameters of different electrospun fiber mats.

3.3 Piezoelectricity: assessing through FTIR and XRD

Fourier transform infrared (FTIR) spectra of the various melt mixed composites and as prepared nanofibers is shown in Fig. 4a and b. As we mentioned in our earlier study,[16] PVDF obtained from an extruder and subsequently compression molded showed a mixture of both α and β-phases; with predominantly α-phase. From the FTIR spectra of neat melt mixed PVDF samples, (Fig. 4a), the characteristic peak at 763 cm^{-1} (CF_2 bending), 975 cm^{-1} (twisting mode of CF_2) confirms the presence of α-phase. In addition, the presence of a small peak at 840 cm^{-1} (CH_2 rocking) indicates the presence of β-phase in PVDF. Neat PVDF as well as PVDF/CNTs composites shows a mixture of both α and β-phases. However, the β-fraction is different in each composite (discussed in later section). Additionally, the presence of C=C– stretching at ~1640 cm^{-1} in PVDF/CNTs composites further confirms the presence of CNTs in the composites.

The spectra of electrospun fibers show the characteristic peaks at 840 cm^{-1} and 1274 cm^{-1} corresponding to the β-phase in the fibers and weak characteristic vibration bands corresponding to 763 cm^{-1} (CH_2 in-plane bending or rocking/CF_2 bending and skeletal bending), 795 (CH_2 rocking), 975 cm^{-1} (CH_2 twisting) indicating the presence of α-phase. Other significant peaks present in PVDF are observed at 877 cm^{-1} (CH_2 out-of-plane bending or rocking) and 976 cm^{-1} (CH_2

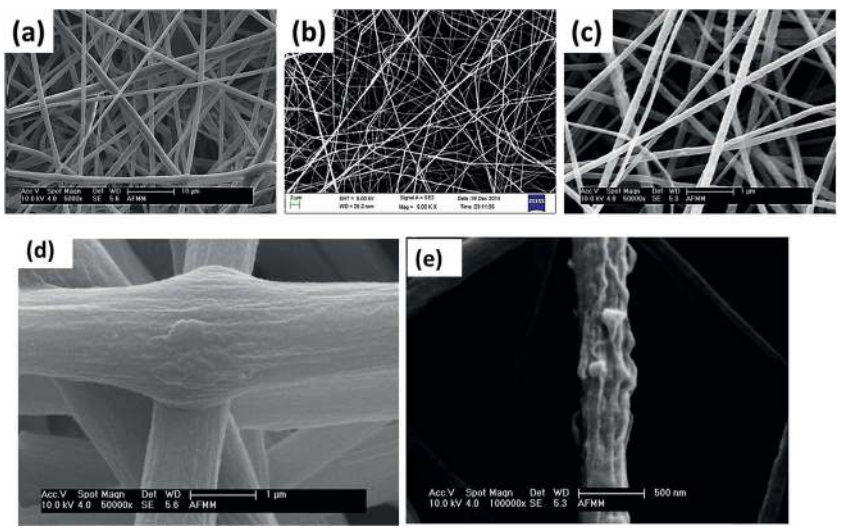

Fig. 2 SEM morphology of (a) PVDF, (b) PVDF/CNT fibers, (c) PVDF/Ag–CNTs (d and e are the high resolution images of PVDF and PVDF/Ag–CNTs fibers respectively).

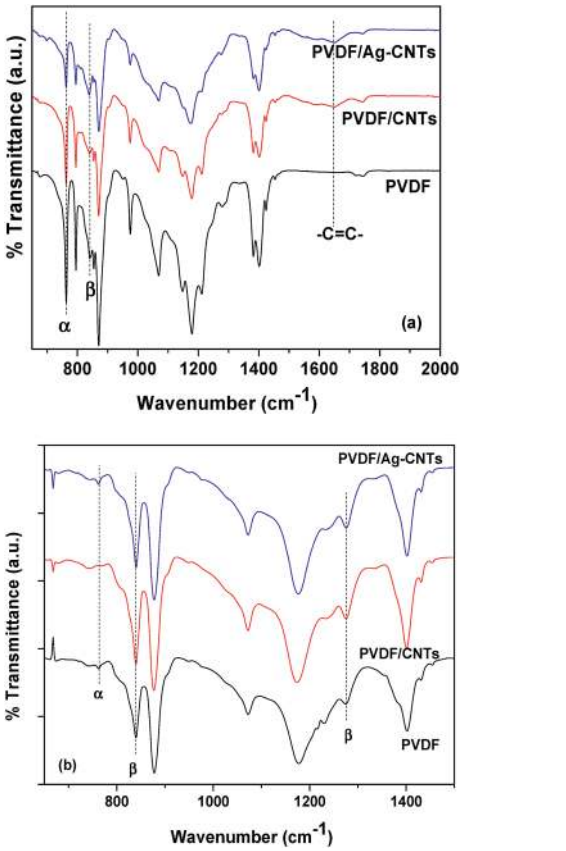

Fig. 4 (a) FTIR spectra of melt mixed composites, PVDF; PVDF/CNTs; PVDF/Ag–CNTs, (b) FTIR spectra of electrospun fibers PVDF; PVDF/CNTs; PVDF/Ag–CNTs.

twisting). The peaks at 840 cm^{-1} and 1274 cm^{-1} corresponds to CH_2 rocking/CF_2 asymmetrical stretching and C–F stretching vibrations of β phase, respectively.[13,46] From FTIR, we can clearly observe that the electrospun fibers predominantly consists of β phase. This establishes that the elongational effect during electrospinning process induces the transformation of α-phase to β-phase in PVDF. It has been reported that the elongation of the jet at the Taylor cone made it easier for the polymer chain orientation along the fiber axis to produce higher content of the polar β-phase.[32]

The β fraction ($F(\beta)$) is further calculated for different fibers from their FTIR spectra using the following equation:[47]

$$F(\beta) = \frac{X_\beta}{X_\alpha + X_\beta} = \frac{A_\beta}{(K_\beta/K_\alpha)A_\alpha + A_\beta} = \frac{A_\beta}{(1.26)A_\alpha + A_\beta}$$

where A_α and A_β are the absorbance values at 763 cm^{-1} and 840 cm^{-1}, respectively. K_α and K_β are the absorption coefficient of the respective wavenumbers ($K_\alpha = 6.1 \times 10^4$ and $K_\beta = 7.7 \times 10^4$ cm^2 mol^{-1}), where X_α and X_β represent the % crystallinity of the α and β phases, respectively. Fig. 5 shows that for the melt mixed composites, $F(\beta)$ increased on addition of nanoparticles. For instance, PVDF shows a β fraction of 0.34 whereas, on addition of Ag–CNTs, the β fraction increases to 0.47. Similar results were obtained by Li *et al.*,[48] where doping of Ag nanowires with PVDF enhances the content of β phase. In this study,

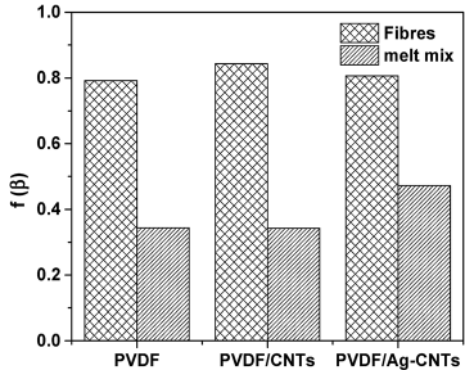

Fig. 5 β fraction ($F(\beta)$) for different types of samples (melt mixed and electrospun fibers) obtained from FTIR data.

the increase in the β phase can be due to interactions between Ag–CNTs and PVDF, which induced the charge accumulation at the surfaces and thereby facilitates the transforms the chain to TTT conformation.[32] This *trans*-conformation can facilitate the nucleation of a polar β phase. Further, the PVDF fibers shows β fraction of 78% that is further increased with the addition of nanoparticles.

The highest β fraction (0.84) is obtained in the case of CNTs filled in PVDF fibers. The FT-IR result indicates that the β fraction in electrospun PVDF/Ag–CNTs fibers is similar to PVDF/CNT fibers. In summary, electrospinning leads to the formation of *trans*-conformation in PVDF, and the extensional flow of the polymer solution under electric field leads to orientation of polymer chains and this is presumably the major factor that helps in the phase transformation.[49]

The FTIR results are further supported by XRD patterns shown in Fig. 6a and b. The melt mixed PVDF samples showed peaks corresponding to α phase at 18.4° (020), 20.0° (110) and a weak shoulder at 20.6° (200) corresponding to the β-phase (Fig. 6a). PVDF/CNTs show similar pattern as that of PVDF whereas in PVDF/Ag–CNTs, a prominent shoulder at 20.6° (200) is observed indicating the presence of higher β-fraction phase in the composite. The XRD scans of the electrospun fibers show a peak at 20.6° ((110) reflection)[16] that indicates the presence of β-phase. On close examination, we find a small hump at 18° indicating the existence of α phase in the electrospun fibers. In our previous study,[35] we have reported that $-NH_2$ functionalized CNTs induces the β-phase in PVDF. It is believed that the specific interactions between the $-NH_2$ groups on the CNTs and the CF_2 dipole of PVDF leads to β-phase in PVDF. Apart from incorporation of nanoparticles, we also demonstrated the use of various processes like mechanical rolling to induce β-phase in the PVDF.[16]

3.4 Dielectric and piezoelectric properties of electrospun fibers

The variation of dielectric constant (ε') as a function of frequency for various composites is shown in Fig. 7. Interestingly, both melt mixed (not shown here) and electrospun fibers show similar trend in dielectric spectroscopy. The dielectric constant of melt mixed PVDF and of electrospun PVDF fibers

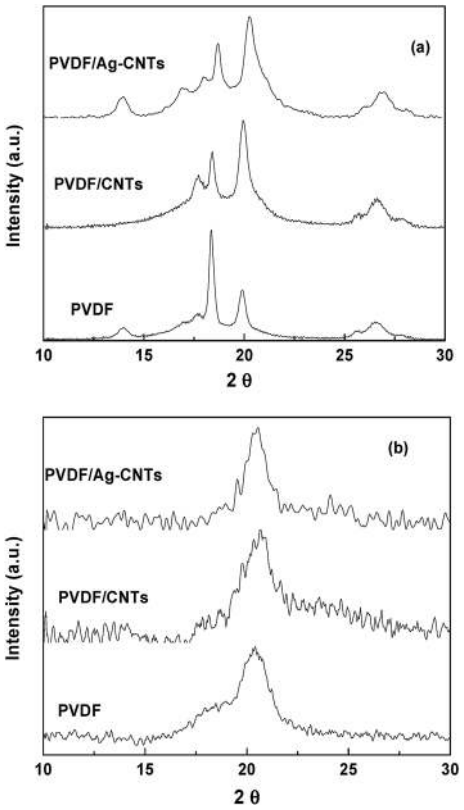

Fig. 6 XRD patterns for (a) melt mixed composites, and (b) electrospun fibers of PVDF nanocomposites.

scales with the addition of both CNTs and Ag–CNTs nanoparticles. For instance, the PVDF fibers showed dielectric permittivity of ~4 (at 100 Hz) which increases with the addition of CNTs (~6 at 100 Hz) and increases sharply for Ag–CNTs (~30 at 100 Hz). The increase in the dielectric constant of the PVDF with the addition of CNTs and with Ag–CNTs is due to the large dielectric permittivity difference between the PVDF matrix and the nanoparticles (CNTs), which causes the accumulation of charge carriers at the interface.[50,51] Although, a direct comparison would be difficult between melt-mixed samples which are solid and electrospun fibers that are porous mat, however, literature reports lower dielectric constants for spun fibers in comparison to melt mixed or solution mixed PVDF samples because of their different degree of porosity.[52] This can be due to high β phase content in the fibers. Similar results were obtained in the studies where increase in β phase content in the PVDF leads to decrease in the dielectric permittivity.[16] A comparison can be carefully made if one can produce porous samples (of the same porosity as that of spun fiber mat) of the melt-mixed samples. However, as the rationale of this study is to understand the effect of various nanoparticles in rendering β-fraction in PVDF, we studied the obtained fibers in more detail using piezoresponse force microscopy and are explained in the next section.

Taken together, it is expected that electrospinning of PVDF can enhance the piezoelectric properties. This can be confirmed by the measurement of the piezoelectric and ferroelectric

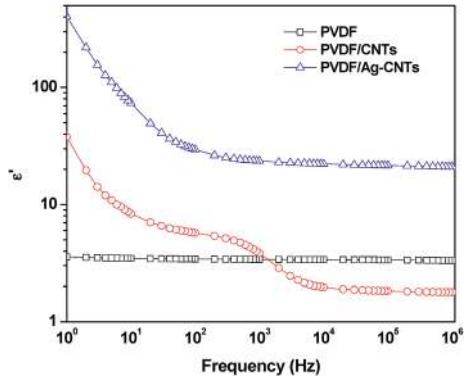

Fig. 7 Dielectric spectra as a function of frequency for electrospun fibers of PVDF nanocomposites.

properties of the electrospun fibers. Piezoresponse force microscopy (PFM) was used to investigate the ferro- and piezoelectric behaviour of neat as well as of composite PVDF fibers. A fiber is said to be piezo- and ferroelectric, if the voltage applied across the fiber induces the structural deformations in the specimen, which is further detected by the PFM probe. Before PFM, we conducted a tapping mode AFM imaging for locating a PVDF fiber. Fig. 8 shows the representative AFM morphologies of different fibers on which PFM was carried out.

The phase obtained from PFM indicates the polarity of the piezoelectric coefficient, whereas the PFM amplitude *vs.* voltage relation corresponds to the strain amplitude. The variation in amplitude is the change of strain under an external field which is a piezoelectric characteristic. The overall alignment of dipoles in the ferroelectric crystallites defines the intensity and shape of the PFM amplitude *versus* voltage loops.[53] It is evident from PFM that electrospun fibers responds to the applied voltage as the applied voltage induces strain within the fiber. This electric field induced strain proves the piezoelectric property of PVDF fibers. The phase switches with external electric field, which is a typical characteristic of a ferroelectric material.[53] PVDF/Ag–CNTs show 180° phase (φ) switching hysteresis loop which is a characteristic of a typical ferroelectric material in switching PFM testing (not shown here). In ferroelectrics, polarization switching occurs at the coercive field which will change the sign of the surface charge, leading to the PFM phase change by 180°.[54] This confirms the ferroelectric and piezoelectric property of neat PVDF fibers as well as nanoparticles filled fibers. By using the amplitude in PFM, we can calculate the total strain S ($S = \Delta t/T$) in the electrospun fibers, where T is the thickness of fiber mat and Δt is the measured change in thickness in the mat. At constant thickness, the strain is higher in PVDF/Ag–CNTs than PVDF/CNTs and PVDF fibers. The observed strain is not merely from piezoresponse, but also can be from different factors like electrostriction, thermal effects and applied pressure in the direction of the electric field.[55] The total strain can be written as;

$$S = S_{\text{piezoelectric}} + S_{\text{electrostriction}} + S_{\text{thermal}} + S_{\text{pressure}} \quad (1)$$

$$S = d_{33}E - QE^2 + \lambda\Delta T + e_{33}\sigma_{33} \quad (2)$$

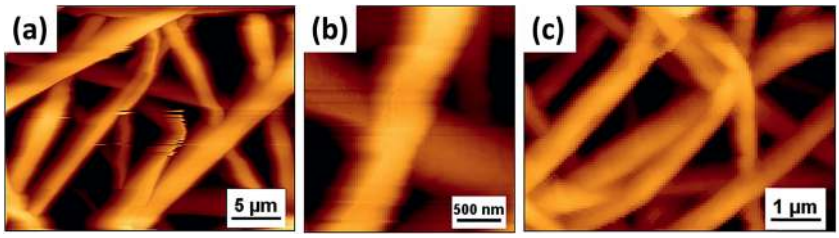

Fig. 8 AFM morphology of (a) PVDF (b) PVDF/CNT fibers, (c) PVDF/Ag–CNTs.

where, d_{33} corresponds to piezoelectric coefficient, E corresponds to electric field, Q is the electrostriction coefficient, λ corresponds to thermal expansion coefficient, ΔT is the change in the temperature, e_{33} is the elastic coefficient and σ_{33} is the stress. As the measurements were performed at room temperature at constant pressure, we can ignore pressure and temperature terms from eqn (2). By eliminating pressure and temperature terms, the eqn (2) becomes,

$$S = d_{33}E - QE^2 \quad (3)$$

An overdetermined system of equations for two unknowns (d_{33} and Q) is obtained, which can be regressed by least-square. Using measured total deflection and applied electric field for 200 data points, we can calculate the d_{33} and Q coefficients from the over-determined system of equations. However, Baji *et al.*[53] showed that d_{33} can directly be calculated using the following equation, as Q is an insignificant term.

$$S = d_{33}E \quad (4)$$

Using the measured data from PFM, d_{33} can be obtained. So the d_{33} can be obtained by amplitude (obtained from PFM) divided by an AC modulation voltage *i.e.* 10 V, in our case. The piezoelectric coefficient for PVDF fibers is *ca.* 30 ± 2 pm V^{-1} and has enhanced with the addition of CNT (35 ± 5 pm V^{-1}) and has drastically increased to 54 ± 5 pm V^{-1} in the presence of PVDF/Ag–CNTs fibers. Our d_{33} values of neat PVDF fibers is in accordance with available literature.[56] The improvement in piezoelectric coefficient with the addition of CNTs is due to high amount of β-phase in the PVDF. It is worth noting that all the PFM measurements were done at very low voltage (−10 to 10 V). It is also very surprising that all electrospun fibers showed almost similar β-fraction but the piezoelectric coefficient is comparatively higher in case of PVDF/CNTs and in Ag decorated CNT incorporated fibers than neat PVDF. Similar results have been reported where addition of CNTs in the PVDF composites leads to high piezoelectric coefficient.[31,32,57] We propose that the presence of Ag decorated CNTs alters the orientation of the dipoles in the PVDF fibers. The incorporation of fillers causes PVDF to swell leading to the formation of extended chain conformation of PVDF around the fillers. Thus, the conformational changes resulting from the inclusion lead to domain rearrangement, which affects the piezoresponse. A table comparing the d_{33} of various PVDF based nanofibers as derived from PFM is shown here. It is well realized that Ag decorated CNTs enhances the d_{33} significantly as compared to other piezoelectric materials like barium titanate under the conditions adopted here (Table 1).

Table 1 Comparison of the piezoelectric coefficient as derived from PFM for various PVDF based nanofibers

Sample	d_{33} value	Reference
PVDF/$BaTiO_3$ fibers	48	53
PVDF nanofibers	57	58
PVDF/Ag–CNTs fibers	54	This work

4. Conclusions

Two different techniques *i.e.* melt mixing and electrospinning were employed to understand the effect of different processes on the structural and piezoelectric properties of PVDF. While both the processes resulted in phase transformation of α- to electroactive β-polymorph in PVDF, the fraction of β-phase induced was strongly dependent on the adopted process. The addition of CNTs and Ag–CNTs facilitates the α- to β-phase transformation in PVDF, as supported by FTIR and XRD. This was attributed to the high electrostatic field that generates extensional forces on the polymer chains which align the dipoles in one direction. The ferroelectric and piezoelectric properties were evaluated by PFM. It was observed that electrospun fibers of PVDF containing Ag decorated CNTs showed the highest piezoelectric coefficient (d_{33} = 54 pm V^{-1}) as compared to CNT containing fibers and control PVDF.

Acknowledgements

Authors would like to acknowledge INSA, India for their financial support. Authors would also like to acknowledge the MNCF facilities at CeNSE and AFMM facilities at IISc.

References

1 R. Gopal, S. Kaur, C. Y. Feng, C. Chan, S. Ramakrishna, S. Tabe and T. Matsuura, *J. Membr. Sci.*, 2007, **289**, 210–219.
2 P. Gibson, H. Schreuder-Gibson and D. Rivin, *Colloids Surf., A*, 2001, **187**, 469–481.
3 H. Fong, W. Liu, C.-S. Wang and R. A. Vaia, *Polymer*, 2002, **43**, 775–780.

4 V. Thavasi, G. Singh and S. Ramakrishna, *Energy Environ. Sci.*, 2008, **1**, 205–221.
5 S. Ramakrishna, K. Fujihara, W.-E. Teo, T. Yong, Z. Ma and R. Ramaseshan, *Mater. Today*, 2006, **9**, 40–50.
6 B. Amrit, M. Sai Rama Krishna, R. Badari Narayana and C. Kaushik, *Nanotechnology*, 2014, **25**, 485101.
7 K. S. Athira, P. Sanpui and K. Chatterjee, *J. Polym. Biopolym. Phys. Chem.*, 2014, **2**, 62–66.
8 W. J. Li, C. T. Laurencin, E. J. Caterson, R. S. Tuan and F. K. Ko, *J. Biomed. Mater. Res.*, 2002, **60**, 613–621.
9 T. T. Wang, Google Patents, US4241128 A, 1980.
10 W. Yasaku and H. Reinosuke, *Jpn. J. Appl. Phys.*, 1976, **15**, 2041.
11 B.-E. El Mohajir and N. Heymans, *Polymer*, 2001, **42**, 5661–5667.
12 A. Richardson, P. S. Hope and I. M. Ward, *J. Polym. Sci., Part B: Polym. Phys.*, 1983, **21**, 2525–2541.
13 A. Salimi and A. Yousefi, *Polym. Test.*, 2003, **22**, 699–704.
14 S. Satapathy, S. Pawar, P. K. Gupta and K. B. R. Varma, *Bull. Mater. Sci.*, 2011, **34**, 727–733.
15 G. T. Davis, J. E. McKinney, M. G. Broadhurst and S. C. Roth, *J. Appl. Phys.*, 1978, **49**, 4998–5002.
16 M. Sharma, G. Madras and S. Bose, *Phys. Chem. Chem. Phys.*, 2014, **16**, 14792–14799.
17 C.-W. Tang, B. Li, L. Sun, B. Lively and W.-H. Zhong, *Eur. Polym. J.*, 2012, **48**, 1062–1072.
18 A. Lund, C. Gustafsson, H. Bertilsson and R. W. Rychwalski, *Compos. Sci. Technol.*, 2011, **71**, 222–229.
19 J. X. Wen, *Polym. J.*, 1985, **17**, 399–407.
20 K. Koga and H. Ohigashi, *J. Appl. Phys.*, 1986, **59**, 2142–2150.
21 M. Sharma, G. Madras and S. Bose, *J. Mater. Chem. A*, 2015, **3**, 5991–6003.
22 A. G. Holmes-Siedle, P. D. Wilson and A. P. Verrall, *Mater. Des.*, 1983, **4**, 910–918.
23 A. M. Vinogradov, V. Hugo Schmidt, G. F. Tuthill and G. W. Bohannan, *Mech. Mater.*, 2004, **36**, 1007–1016.
24 L. Mateu and F. Moll, in *Review of Energy Harvesting Techniques and Applications for Microelectronics (Keynote Address)*, 2005, pp. 359–373.
25 H. Lee, R. Cooper, K. Wang and H. Liang, *Sensors*, 2008, **8**, 7359.
26 S. Manna, S. K. Batabyal and A. K. Nandi, *J. Phys. Chem. B*, 2006, **110**, 12318–12326.
27 E. S. Cozza, O. Monticelli, E. Marsano and P. Cebe, *Polym. Int.*, 2013, **62**, 41–48.
28 Z. Zhao, J. Li, X. Yuan, X. Li, Y. Zhang and J. Sheng, *J. Appl. Polym. Sci.*, 2005, **97**, 466–474.
29 J. R. Kim, S. W. Choi, S. M. Jo, W. S. Lee and B. C. Kim, *Electrochim. Acta*, 2004, **50**, 69–75.
30 S. W. Choi, S. M. Jo, W. S. Lee and Y. R. Kim, *Adv. Mater.*, 2003, **15**, 2027–2032.
31 Z. H. Liu, C. T. Pan, L. W. Lin and H. W. Lai, *Sens. Actuators, A*, 2013, **193**, 13–24.
32 Y. Ahn, J. Y. Lim, S. M. Hong, J. Lee, J. Ha, H. J. Choi and Y. Seo, *J. Phys. Chem. C*, 2013, **117**, 11791–11799.
33 S. Theron, E. Zussman and A. Yarin, *Polymer*, 2004, **45**, 2017–2030.
34 P. Heikkilä and A. Harlin, *Eur. Polym. J.*, 2008, **44**, 3067–3079.
35 M. Sharma, K. Sharma and S. Bose, *J. Phys. Chem. B*, 2013, **117**, 8589–8602.
36 J. D. Kim, H. Yun, G. C. Kim, C. W. Lee and H. C. Choi, *Appl. Surf. Sci.*, 2013, **283**, 227–233.
37 K. Ketpang and J. S. Park, *Synth. Met.*, 2010, **160**, 1603–1608.
38 Z.-M. Huang, Y. Z. Zhang, M. Kotaki and S. Ramakrishna, *Compos. Sci. Technol.*, 2003, **63**, 2223–2253.
39 S. V. Fridrikh, H. Y. Jian, M. P. Brenner and G. C. Rutledge, *Phys. Rev. Lett.*, 2003, **90**, 144502.
40 M. G. McKee, G. L. Wilkes, R. H. Colby and T. E. Long, *Macromolecules*, 2004, **37**, 1760–1767.
41 S. W. Choi, J. R. Kim, Y. R. Ahn, S. M. Jo and E. J. Cairns, *Chem. Mater.*, 2007, **19**, 104–115.
42 L. Y. Yeo and J. R. Friend, *J. Exp. Nanosci.*, 2006, **1**, 177–209.
43 K. Pilehrood Mohammad, P. Heikkilä and A. Harlin, *Autex R. J.*, 2012, **12**, 1.
44 S. Mazinani, A. Ajji and C. Dubois, *Polymer*, 2009, **50**, 3329–3342.
45 Y. Cai, X. Xu, C. Gao, L. Wang, Q. Wei, L. Song, Y. Hu, H. Qiao, Y. Zhao, Q. Chen and H. Fong, *Fibers Polym.*, 2012, **13**, 837–845.
46 Y. Bormashenko, R. Pogreb, O. Stanevsky and E. Bormashenko, *Polym. Test.*, 2004, **23**, 791–796.
47 J. R. Gregorio and M. Cestari, *J. Polym. Sci., Part B: Polym. Phys.*, 1994, **32**, 859–870.
48 B. Li, C. Xu, J. Zheng and C. Xu, *Sensors*, 2014, **14**, 9889.
49 Y.-L. Liu, Y. Li, J.-T. Xu and Z.-Q. Fan, *ACS Appl. Mater. Interfaces*, 2010, **2**, 1759–1768.
50 S. Maya, S. Ranganatha, K. Ajay Kumar, R. Rajeev, M. Giridhar and B. Suryasarathi, *Mater. Res. Express*, 2014, **1**, 045301.
51 M. Sharma, M. P. Singh, C. Srivastava, G. Madras and S. Bose, *ACS Appl. Mater. Interfaces*, 2014, **6**, 21151–21160.
52 R. Gregorio Jr and E. Ueno, *J. Mater. Sci.*, 1999, **34**, 4489–4500.
53 A. Baji, Y.-W. Mai, Q. Li and Y. Liu, *Compos. Sci. Technol.*, 2011, **71**, 1435–1440.
54 M. Hongchen, T. Chi, Z. Xilong, W. Xiaoyong and L. Faxin, *Europhys. Lett.*, 2014, **108**, 27010.
55 M. Kanik, O. Aktas, H. S. Sen, E. Durgun and M. Bayindir, *ACS Nano*, 2014, **8**, 9311–9323.
56 N. Soin, D. Boyer, K. Prashanthi, S. Sharma, A. A. Narasimulu, J. Luo, T. H. Shah, E. Siores and T. Thundat, *Chem. Commun.*, 2015, **51**, 8257–8260.
57 G. H. Kim, S. M. Hong and Y. Seo, *Phys. Chem. Chem. Phys.*, 2009, **11**, 10506–10512.
58 J. Pu, X. Yan, Y. Jiang, C. Chang and L. Lin, *Sens. Actuators, A*, 2010, **164**, 131–136.

